

SCIENTIFIC REPORTS



OPEN

Significant discharge of CO₂ from hydrothermalism associated with the submarine volcano of El Hierro Island

Received: 21 October 2015

Accepted: 21 April 2016

Published: 09 May 2016

J. M. Santana-Casiano¹, E. Fraile-Nuez², M. González-Dávila¹, E. T. Baker³, J. A. Resing³ & S. L. Walker⁴

The residual hydrothermalism associated with submarine volcanoes, following an eruption event, plays an important role in the supply of CO₂ to the ocean. The emitted CO₂ increases the acidity of seawater. The submarine volcano of El Hierro, in its degasification stage, provided an excellent opportunity to study the effect of volcanic CO₂ on the seawater carbonate system, the global carbon flux, and local ocean acidification. A detailed survey of the volcanic edifice was carried out using seven CTD-pH-ORP tow-yo studies, localizing the redox and acidic changes, which were used to obtain surface maps of anomalies. In order to investigate the temporal variability of the system, two CTD-pH-ORP yo-yo studies were conducted that included discrete sampling for carbonate system parameters. Meridional tow-yos were used to calculate the amount of volcanic CO₂ added to the water column for each surveyed section. The inputs of CO₂ along multiple sections combined with measurements of oceanic currents produced an estimated volcanic CO₂ flux = $6.0 \cdot 10^5 \pm 1.1 \cdot 10^5 \text{ kg d}^{-1}$ which is ~0.1% of global volcanic CO₂ flux. Finally, the CO₂ emitted by El Hierro increases the acidity above the volcano by ~20%.

The knowledge and quantification of heat and chemicals fluxes from vent fields requires information about the hydrothermal discharges in these systems. Hydrothermal vents discharge discrete jets of undiluted high-temperature fluids or diffuse seepage of low-temperature diluted fluids¹. Although most research has been concerned with discrete discharge, some studies have focused on diffuse emissions². Data on the magnitude of diffuse flow and its role in geochemical fluxes to the global ocean are limited^{1,3-7}. However, it has been suggested that the geochemical influence of low-temperature diffuse flow to the global ocean could exceed that of high-temperature flow⁸. Although hydrothermalism is commonly associated with volcanic islands, coastal and shallow hydrothermal systems are still poorly studied compared to deep-water mid-ocean ridge systems. The existence of shallow submarine hydrothermal venting has been revealed by the presence of streams of gas bubbles off volcanic islands⁹ such as White Island, (New Zealand)¹⁰⁻¹¹, Papua New Guinea¹², Iceland¹³, Milos, Greece¹⁴, Panarea, (Italy)¹⁵, and the Azores⁹.

Studies of hydrothermal activity on submarine volcanoes along volcanic arcs also reveal a great diversity of hydrothermal activity¹⁶ at sites such as NW Eifuku¹⁷, NW Rota-1^{18,19}, and Suiyo Seamount²⁰. Investigations have also been carried out on hydrothermal activity associated with intra-plate volcanoes, including the Society Islands²¹, Hawaii²², Loihi²³, and Vailulu'u²⁴.

Submarine volcanoes exhibit a wide range of CO₂ to pH relationships, from the venting of acid-rich fluids, to CO₂-rich fluids, to fluids rich in alkalinity and CO₂¹⁹. The shallow depths of many of these volcanoes result in the emplacement of their volcanic and hydrothermal products into the surface oceans where they influence surface ocean chemistry and productivity. However, in places where gas bubbles or hot plumes are not easily observed,

¹Instituto de Oceanografía y Cambio Global (IOCG). Universidad de Las Palmas de Gran Canarias. Las Palmas de Gran Canaria. Spain. ²Instituto Español de Oceanografía. Centro Oceanográfico de Canarias. 38180 Santa Cruz de Tenerife. Spain. ³Joint Institute for the Study of the Atmosphere and Ocean, University of Washington, and Pacific Marine Environmental Laboratory, NOAA, Seattle WA, USA. ⁴Pacific Marine Environmental Laboratory, NOAA, Seattle WA, USA. Correspondence and requests for materials should be addressed to J.M.S.-C. (email: magdalena.santana@ulpgc.es)

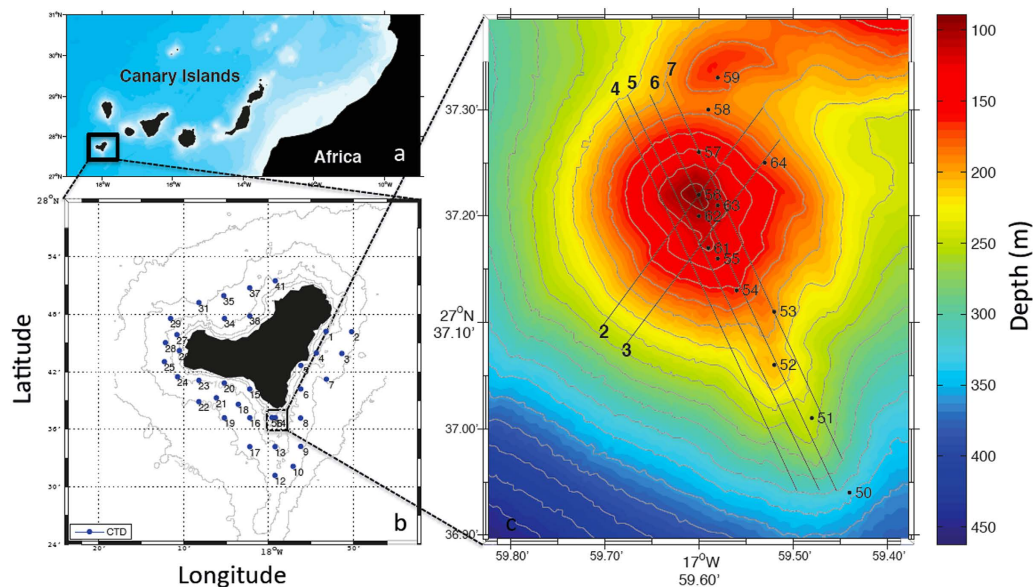


Figure 1. (a) Location of El Hierro volcanic edifice within the Canary Archipelago. (b) Island of El Hierro and the stations sampled. (c) Location of the tow-yos and CTD stations. The maps were generated using Matlab 7.12 R2011a.

the detection and sampling of emissions, either discrete or diffuse, is required to evaluate the magnitude of a volcano's contribution to the global budget of gas emissions.

Here we present a study of chemical anomalies associated with hydrothermal emissions in the shallow waters around the submarine volcano of El Hierro. Oxidation-Reduction Potential (ORP) and pH sensors were used in combination with a Conductivity-Temperature-Depth (CTD) package in tow-yo surveys in order to define the area affected by the hydrothermal emissions and to obtain a map of ORP and pH anomalies. In addition, we conducted a temporal study on variations of the physical-chemical properties within the plumes related to physical processes. Together, these data provided a direct constraint on the role played by CO₂ emissions from the hydrothermal activity associated with volcanic islands and their contribution to ocean acidification. These data comprise the first detailed survey of pH and ORP around the summit of a shallow submarine volcano.

Regional Setting

The Canary Islands, off northwest Africa (Fig. 1a), were constructed in the Early Miocene as the African plate moved over a mantle hotspot²⁵. The islands show a general age progression from the eastern islands (>20 Ma) toward El Hierro (<2 Ma)²⁶. The oldest subaerial rocks in El Hierro have been dated at 1.12 ± 0.02 Ma²⁷. This island is the emergent summit of a volcanic shield that rises from 3800–4000 m depth and grows up to 1500 m above sea level. The subaerial part (280 km²) includes three convergent volcanic rifts (NE-Rift, NW-Rift and S-Rift)²⁸. Sedimentary relicts from the 2011 El Hierro eruption demonstrate unequivocally that the youngest pre-island sediment is located beneath El Hierro thereby providing crucial support for an east-west age progression of the onset of volcanism in the Canary archipelago. The fossil evidence from El Hierro therefore concludes the current debate on the origin of the Canary Islands and reinstates a mantle-plume as the most plausible cause of volcanism in the Canary Islands²⁹.

The submarine volcano of El Hierro is located 1.8 km south of the Island of El Hierro (Fig. 1a,b). The submarine volcano begins on the S-Ridge at 350 m depth and rises up to 88 m below sea level. It was erupting molten material for five months from October 2011 to March 2012, changing drastically the physical-chemical properties of the water column in the area. After this eruption, the system evolved to hydrothermal vents^{30,31}.

Survey of the volcanic edifice

The production of a hydrothermal emission map of the El Hierro edifice required a detailed survey of the area that was carried out through a tow-yo study. From the base to the top of the submarine volcano, an instrument package was towed in a sawtooth pattern by continual lowering and raising between 3 m and 40 m above the seafloor. To delimit the area of anomalies due to hydrothermal emissions, seven SeaBird 911 + CTD-pH-ORP tow-yos were carried out in the area. Four parallel tow-yos followed the topography of the principal and secondary cones and another two tow-yos were perpendicular to these. Tow-yo 6 repeated tow-yo 1 (Fig. 1c). In order to investigate the temporal variability of the system, two CTD-pH-ORP yo-yo studies (raising and lowering the CTD at one location) were carried out from the surface to 3 m above the seabed at two stations (st. 56 and st. 61, Fig. 1c) with 38 and 61 casts, respectively. The time between each cast was 10 minutes and the total duration of the yo-yo study was 6 hours for st. 56 and 10 hours for st. 61. For station 61, three water column sampling casts for discrete pH, total alkalinity (A_T) and total dissolved inorganic carbon (C_T) were carried in the maximum anomalies detected with the temperature (T), ORP, and pH sensors. Additionally, 50 stations were occupied around the island of El Hierro outside of the volcano's influence.

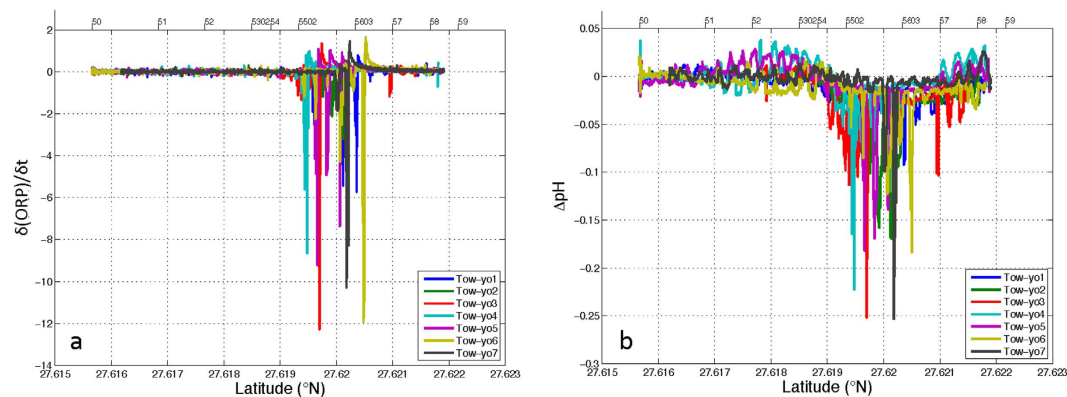


Figure 2. Plots of (a) $\delta(\text{ORP})/\delta t$ and (b) ΔpH versus latitude obtained from tow-yos 1–7.

Use of ORP and pH sensors to detect changes in the redox and acid-base properties of seawater

The detection of emissions from low-temperature hydrothermal vents, where the increase in temperature is not evident, requires the utilization of alternative sensors that respond to emissions of certain chemical species. The character of both reduced and acid fluids in the volcanic emissions in the El Hierro submarine volcano³¹ allowed us to detect anomalies related with changes in the chemical potential and the proton concentration using ORP and pH sensors, respectively. Tow-yos with these sensors provided the approximate locations of the emissions as can be seen in the plot of $\delta(\text{ORP})/\delta t$ and ΔpH versus the latitude (Fig. 2). The ORP sensor responds very quickly to the presence of reduced chemicals in the water column. Changes in potential are proportional to the amount of reduced chemical species present in the water. Here we examine the magnitude of this change by the time derivative of ORP, $\delta(\text{ORP})/\delta t$. For pH changes, the mean pH for each depth at a reference station in an area not affected by the vent emission was subtracted from each point measured near the volcanic edifice, defining in this way ΔpH . The signal of the two sensors differs because they respond to different chemical processes. The ORP sensor detects changes in the electrochemical potential due to the emission of reduced species (equation 1) and the pH sensor responds to changes in the H^+ concentration due to both CO_2 and acid emissions (equation 2)



where *Red* refers to reduced species (Fe^{+2} , HS^- and H_2), and AH_n refers to acidic compounds (HCl, CO_2 , etc).

Results

Delimiting the seawater volume affected by hydrothermal emissions. Anomalies in pH and ORP measurements followed the same pattern in latitude (Fig. 2) and longitude, which indicates that the emissions of both acid and reduced components must be produced in the same area. Although this study was carried out two years after the eruption of molten material had ceased and a degasification phase had begun³¹, the negative pH anomalies observed in the area, including values as high as -0.25 , cannot be explained by the arrival of water from the surrounding depths. The pH value of 7.89 in the volcano area is found in the non-affected surrounding water at a depth of 900 m. Moreover, the ORP sensor detected changes that can only be explained by the presence of reduced species due to the existence of vents because this is an area of open waters and its potential must correspond to that of an oxic environment. Hydrothermal ORP anomalies are generally restricted to within ~ 1 km of their source because of the rapid oxidation of the reduced species³².

Anomalies of both pH and ORP obtained during the 7 tow-yos over the volcano provided a contour map of the affected surface. In order to quantify this surface, two longitudinal (2–3) and four meridional (4–7) tow-yo sections were used. Using a Mat lab routine and considering that the pH anomalies should be higher than -0.04 , the affected area was $13,000 \pm 800 \text{ m}^2$. The volume, $206,000 \pm 50,000 \text{ m}^3$, was calculated considering the real contoured affected area in each tow-yo transect (i.e., between 3 and 40 m above bottom).

Using a shipboard Acoustic Doppler Current Profiler (ADCP) during the tow-yos over the volcanic edifice, mean velocities, perpendicular to each transect, were calculated for each tow-yo (0.22 , 0.17 , 0.22 and 0.21 cm s^{-1} , respectively for tow-yos 4–7), with a mean velocity = $0.20 \pm 0.12 \text{ cm s}^{-1}$. Figure 3 shows the current speed and direction for tow-yos 4–7. The current direction was to the south-southwest and was relatively stable for all tow-yos. The tide was not eliminated from the data in order to show that its effect, compared with the predominant direction and intensity of the main current, does not change the direction of the resultant velocity.

Estimation of the CO_2 flux from the volcanic edifice. Repetitive yo-yos at stations 56 and 61 confirm significant emissions of CO_2 from the volcano and indicate a significant fluctuation in the carbon system variables (in pH and in both C_T and A_T when measured) associated mostly with changes in local currents. The yo-yo studies carried out at station 61 (Fig. 4a,b) and 56 (Fig. 4c,d) showed that changes in the current intensity and direction produced a discontinuous signal in pH and $\delta(\text{ORP})/\delta t$. St. 56 is located at the top of the cone and st. 61 on one

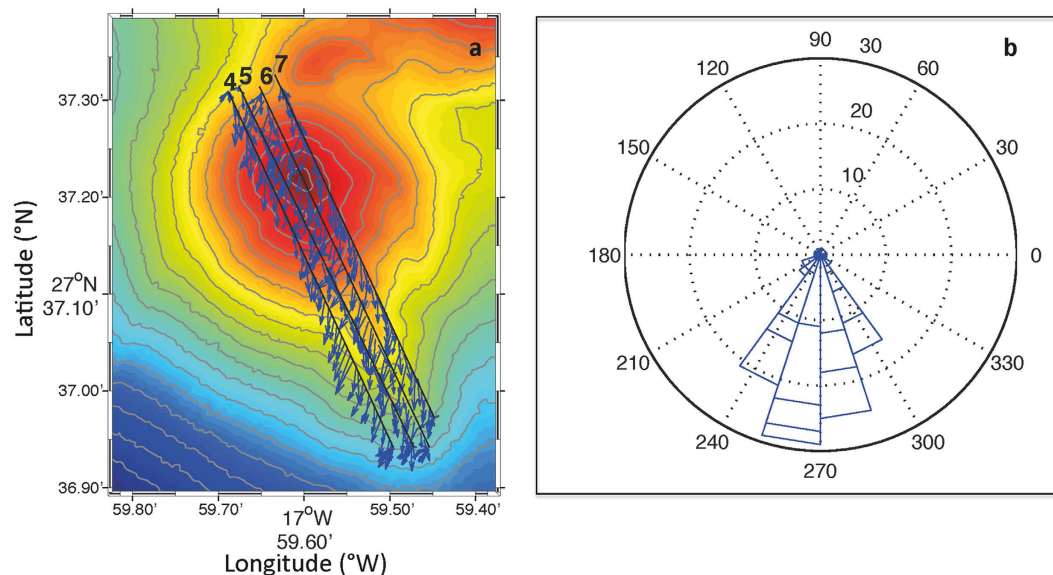


Figure 3. (a) ADCP mean average (cm/s) and (b) ADCP mean direction for all meridional tow-yo transects carried out on 21st March 2014.

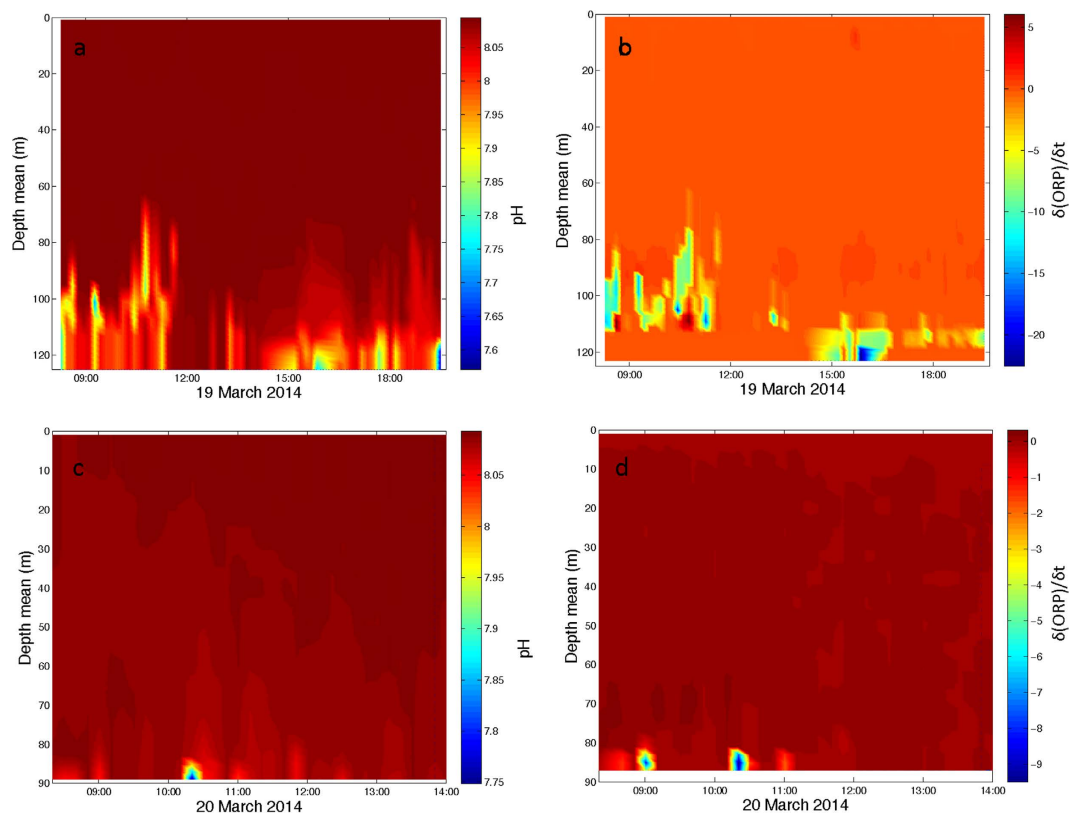


Figure 4. Yo-yo studies carried out at station 61 for (a) pH and (b) $\delta(\text{ORP})/\delta t$ and station 56 for (c) pH and (d) $\delta(\text{ORP})/\delta t$.

of the flanks. During the yo-yo studies, higher anomalies were observed at st. 61 than at st. 56. Figure 5 shows both the intensity and direction of the current for yo-yo 61. For the first 6–8 hrs of yo-yo sampling little variation in current direction or velocity was observed. The tidal mode at this site is M2, with a period of 12 hours and negligible velocity relative to the predominant local mean current³³. However, an increase in the velocity of the zonal component in the second half of the record could explain the pattern of the anomalies observed in Fig. 4a,b. When current velocity was low, as during the first hours of the study, the anomalies were greater than when the current velocity intensity increased.

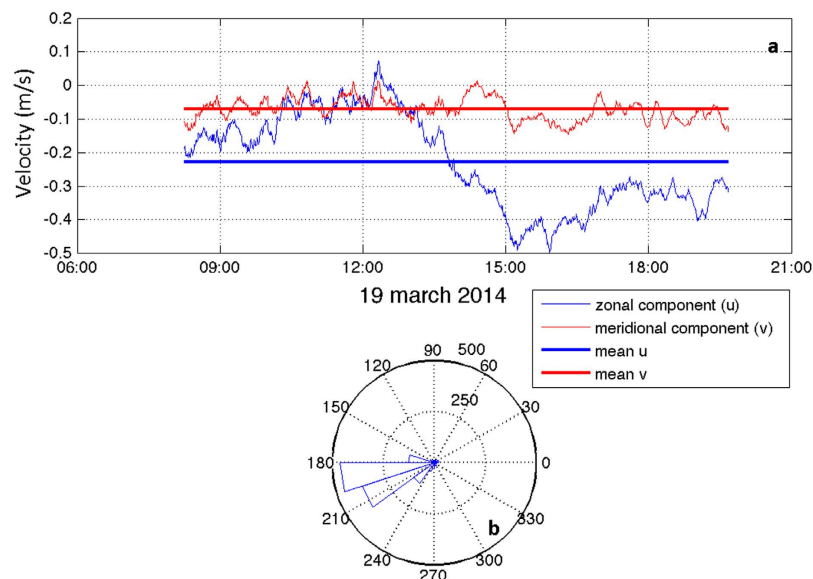


Figure 5. (a) ADCP meridional and zonal components of the velocity and (b) ADCP mean direction for the yo-yo 61 station.

At st. 61, discrete samples were taken at three different times when the sensors registered the highest anomalies in order to measure pH, alkalinity, and total dissolved inorganic carbon. For these three variables, anomalous values were found close to the bottom. pH values were lower than those expected at this depth, and C_T and A_T values higher than usual. C_T and A_T were then normalized to a constant salinity ($NX_T = (X_T/S) \cdot 36.5$) in order to avoid the salinity effect due to the possible advection of different water masses. The normalized values showed the anomalies were not removed (Fig. 6). On yo-yo 6142, the NC_T increased from $2100 \mu\text{mol kg}^{-1}$ to $2400 \mu\text{mol kg}^{-1}$ and the NA_T from $2390 \mu\text{mol kg}^{-1}$ to $2520 \mu\text{mol kg}^{-1}$, at a depth of 120 m, close to the bottom, indicating that the hydrothermal fluid producing these changes was $\sim 57\%$ CO_2 and 43% carbonate alkalinity (HCO_3^- , CO_3^{2-}). The same was observed for yo-yos 6137 at 120 m depth and 6161 between 110 and 120 m depth, but to a lesser degree. The decreases in pH of 0.08, 0.25, and 0.34 units for three yo-yos (Table 1) were therefore the result of the injection of a fluid rich in both carbonate alkalinity and CO_2 gas. This is further supported by the linear relationship between ΔC_T and ΔpH obtained from the data in Table 1 following Resing *et al.*¹⁹, which has a slope of -842 ± 35 ($r^2 = 0.982$). If only CO_2 is added, the slope of ΔC_T versus ΔpH is approximately $334 \mu\text{mol kg}^{-1}/\text{pH}$ unit (Supplementary Fig. S1). The slope of -842 arises from the addition of a hydrothermal source fluid rich in CO_2 and carbonate alkalinity in a ~ 60 – 40% ratio. Figure 6 shows that the emissions of this hydrothermal area acted as an irregular source of CO_2 (Table 1). The corresponding changes in pH varied from 0.082 to 0.344 due to the increase in the proton concentration. The total proton concentration increased between 20% (cast 6137) and 120% (cast 6142), strongly contributing to acidifying the system.

Distribution maps of the surface affected by the emissions can be obtained from the anomalies of ORP, pH, or T observed in the tow-yo sections. In order to compute the equivalent anomalies for C_T over the seven tow-yo sections measured with the sensors the next procedure was followed. Firstly, an equation for the C_T reference (C_T reference = $2109.66 + 0.042x + 5.35 \cdot 10^{-4}x^2 - 7.81 \cdot 10^{-7}x^3$, $r^2 = 0.994$, where x = depth) was obtained using the measured discrete C_T data from 38 stations over the upper 500 m around the El Hierro Island (Fig. 1b). Secondly, a linear relationship between ΔpH (pH *in situ* volcano – pH *in situ* reference) and ΔC_T (C_T volcano – C_T reference) was determined ($\Delta C_T = -893.4 \Delta\text{pH}$, $r^2 = 0.999$) using all the discrete samples of station 61, including the highest, lowest and non-anomalous values. Through this linear relationship the ΔpH calculated using the pH sensor for the tow-yo sections was transformed to the equivalent ΔC_T .

From a surface map of ΔC_T (Fig. 7) it seems that the hydrothermal discharge occurs from a multitude of vents dispersed around the main cone, mainly in two areas (A1 and A2). In these areas, we suggest that the flow is dominated by percolation of vent fluids through the new, highly permeable volcanic edifice. The scale of the anomalies was highly variable near the main cone and the anomaly found in the position of st. 61 during the tow-yo study was not the highest but rather an intermediate anomaly compared with values determined during the yo-yo. The integrated carbon along each tow-yo section was computed and plotted. (Supplementary Fig. S2 shows the anomalies of C_T meridional contours and Supplementary Fig. S3 shows the anomalies of C_T in the zonal contours.)

Using contours from tow-yos 4–7 (Supplementary Fig. S2) the fluxes of the anomalies in C_T were calculated for each tow-yo using the observed anomaly area for every contour, the average anomalies of C_T , and the current speed normal to the tow-yos for each tow-yo. The average flux of CO_2 for these four tow-yos is $6.0 \cdot 10^5 \pm 1.1 \cdot 10^5 \text{ kg d}^{-1}$ for the whole volume. The same calculation can be carried out for each of tow-yos 4–7 to estimate the variations in the proton concentration. We estimate that the excess CO_2 in all the affected volume of $206,000 \pm 50,000 \text{ m}^3$ around the volcano produced an integrated 20% increase in seawater acidity.

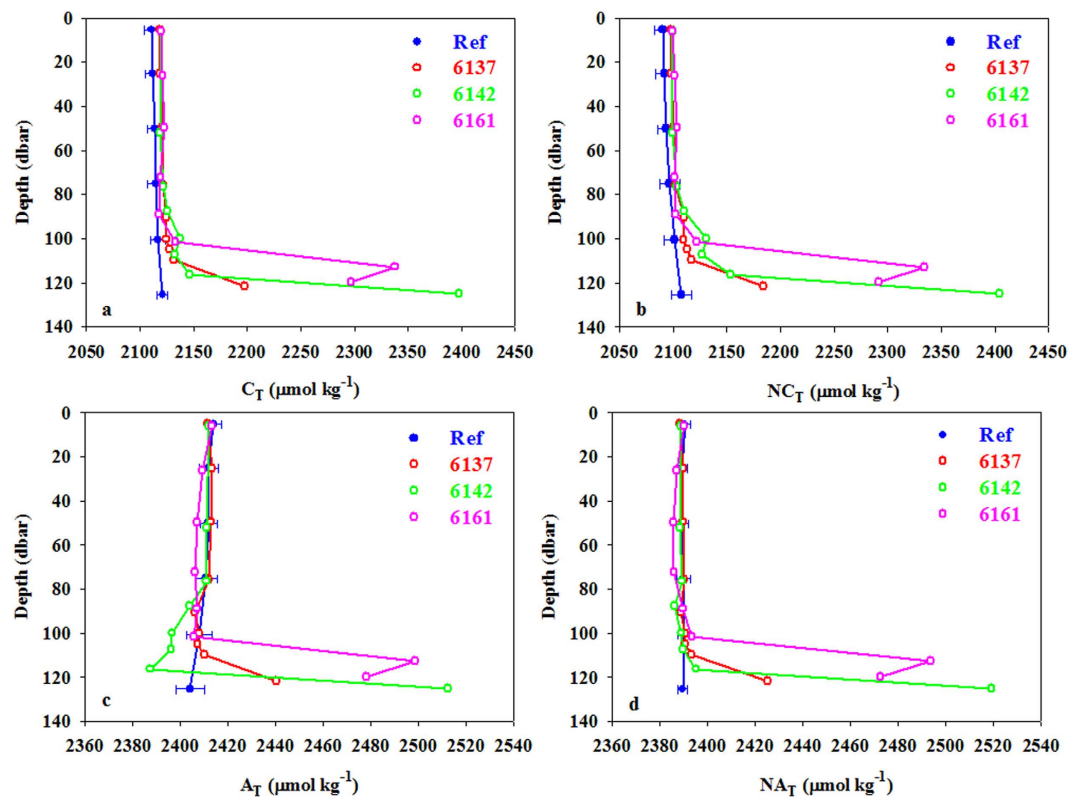


Figure 6. Carbonate variables, (a) C_T , (b) NC_T , (c) A_T and (d) NA_T , expressed in $\mu\text{mol kg}^{-1}$ at station 61, taken at three different yo-yos (37, 42 and 61) for the yo-yo series. NC_T and NA_T were normalized at a constant salinity of 36.5.

Station-cast	6137	6142	6161	6161
Depth (m)	121	125	113	120
T (°C)	18.3838	16.8415	17.8663	17.8615
S	36.7198	36.3735	36.5994	36.5529
Ref C_T	2120.5	2121	2119.1	2120.2
ΔC_T	77.3	276.8	219.2	176.7
Ref A_T	2404.6	2404	2406	2404.9
ΔA_T	35.7	108.3	92.6	73.1
Ref pH	8.078	8.077	8.081	8.079
ΔpH	-0.082	-0.344	-0.25	-0.201
Ref $f\text{CO}_2$	371.6	372.5	369.1	371.1
$\Delta f\text{CO}_2$	101.3	595.2	382.6	288.4

Table 1. Differences with respect to the reference values (regional backgrounds) (Ref) for C_T , A_T , pH and $f\text{CO}_2$ for cast 37, 42 and 61 expressed as ΔC_T , ΔA_T , ΔpH and $\Delta f\text{CO}_2$, respectively. T and S are the values for each station at each depth.

Summary and Discussion

The tow-yo studies carried out around El Hierro submarine volcano showed that the anomalies in ORP and pH followed the same pattern in latitude and longitude. Surface maps of anomalies can be defined from these properties and also from the calculated C_T . The anomalies are all concentrated in a surface area of $13000 \pm 800 \text{ m}^2$ around the main cone of the volcano (area A1 in Fig. 7). This indicates that anomalies of both acid and reduced components must be produced by the hydrothermal emissions of the volcano and not by upwelling water from the surrounding depths. Measurements of the local current velocities support this conclusion. Moreover, from the yo-yo studies, variability in the strength of the emission anomalies is explained by a change in the velocity of the current.

The acidic emissions from the volcanic edifice produced a CO_2 flux of $6.0 \cdot 10^5 \pm 1.1 \cdot 10^5 \text{ kg d}^{-1}$, primarily transported to the southwest. This flux is comparable to that determined from NW Rota-1 ($\sim 1 \pm 0.25 \cdot 10^6 \text{ kg d}^{-1}$), an erupting submarine volcano in the Mariana arc³⁴. The global volcanic flux of CO_2 is estimated³⁵ to be $\sim 7.2 \cdot 10^8 \text{ kg d}^{-1}$

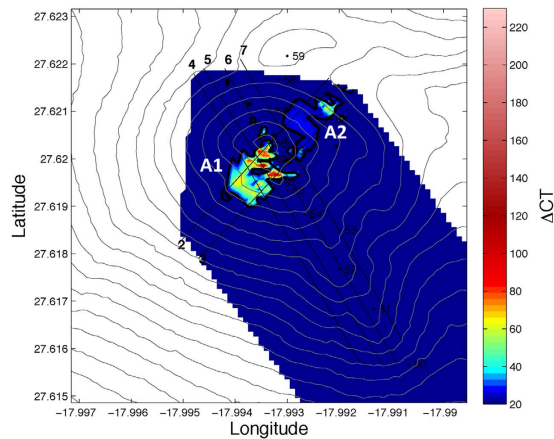


Figure 7. Distribution map of ΔC_T showing areas presumably affected by diffuse venting. Principal and secondary affected areas are labelled as A1 and A2, respectively. The map was generated using Matlab 7.12 R2011a.

considering mid-ocean ridges, arcs and plumes. These emissions also alter the balance of protons in the surrounding ocean, decreasing pH by ~ 0.25 – 0.30 units and increasing the seawater acidity by $\sim 20\%$.

Emissions of CO_2 gas and carbonate alkalinity from El Hierro accounted for 60% and 40%, respectively, of the pH change in local seawater. When both CO_2 and carbonate alkalinity are added, pH decreases, but the decrease is less than when only CO_2 is added. These results are in agreement with previous studies in which carbonate alkalinity from diffuse low-temperature venting accounted for 20% to 40% of the changes observed in pH at submarine volcanoes Ruby, Maug, and Esmeralda¹⁹.

Sites like these provide an excellent opportunity to study the carbonate system, the volcanic contribution to the global volcanic carbon flux, and the potential environmental impact of these emissions on the surrounding ocean. The flux of CO_2 from El Hierro submarine volcano ($6.0 \cdot 10^5 \pm 1.1 \cdot 10^5 \text{ kg d}^{-1}$) is comparable to that at other submarine volcanoes³⁴ but relatively small compared to both the global volcanic flux of CO_2 ³⁵ ($\sim 0.1\%$) and the anthropogenic flux³⁶ ($\sim 0.002\%$). Although CO_2 flux data from hydrothermally and volcanically active submarine volcanoes in the ocean are scarce, it is estimated that mid-ocean ridge, arcs and plumes contribute³⁵ with $2.7 \cdot 10^8 \text{ kg d}^{-1}$, $3.0 \cdot 10^8 \text{ kg d}^{-1}$ and $3.6 \cdot 10^8 \text{ kg d}^{-1}$, respectively. Each of them provides $0.1 \pm 0.02 \text{ Gt of CO}_2 \text{ yr}^{-1}$ to the total CO_2 added to the ocean. More importantly, however, the emission of CO_2 from submarine volcanoes generates local ocean acidification that could affect biological communities, with especially important consequences for organisms that use calcium carbonate in their structures.

Methods

Hydrographic stations were carried out from surface to 1200 m depth with a SeaBird 911+ CTD (Conductivity-Temperature-Depth) with redundant sensors for temperature and conductivity together with light transmission (Chelsea/Seatech), dissolved oxygen (SBE 43), pH (SBE 18), ORP (Oxidation-Reduction-Potential, PMEL-NOAA), pressure, and altimeter sensors. The accuracy of the temperature and conductivity sensors are $0.001 \text{ }^\circ\text{C}$ and 0.0003 S/m , respectively. Water samples with a 24–12L bottle carousel were carried out at 52 stations for the measurements of O_2 , pH, A_T and C_T . A high-resolution study over the submarine volcano including hydrographic station 50–59 and 61–64 was done. Moreover, 3 yo-yos (over stations 54, 56 and 61) and 7 tow-yos using CTD including the pH and ORP sensors were conducted over the volcanic edifice. Yo-yos and tow-yos are effective methods for mapping and sampling hydrothermal plumes. Both operations consisted in lowering the CTD package to near the bottom, then with the ship in the same position for the yo-yo and with the ship moving for the tow-yo, cycling the package up and down only through the bottom few hundred meters. R/V *Ángeles Alvariño*, from the Spanish Institute of Oceanography, used a Dynamic Positioning System to conduct tow-yos at 0.2–0.4 kn.

ADCP. Continuous current measurements were made in the upper waters using a 150 kHz Ocean Surveyor Shipboard Acoustic Doppler Current Profiler, SADC. The ADCP provides estimates of the horizontal velocity components as a function of depth, based on the Doppler effect of sound wave reflections against small particles carried by ocean currents. Such velocity profiles are obtained approximately every second and averaged over 5 minutes and binned vertically in 8 m increments.

pH sensor. The SBE 18 pH sensor uses a pressure-balanced glass-electrode/Ag/AgCl-reference pH probe to provide *in-situ* measurements at depths up to 1200 meters. The sensor was initially calibrated against buffer solutions (4, 7, and 10 pH ± 0.02 pH) following the Sea-Bird protocol. In order to express the measurements in total pH scale, all the data were corrected. For this, discrete values of pH, at fixed depth, from the sensor ($\text{pH}_{\text{NBS in situ}}$) were compared with the pH of samples measured in the water column using the m-cresol purple methods for UV-vis spectrophotometric pH ($\text{pH}_{\text{T in situ}}$) obtaining a dependence equation $\text{pH}_{\text{T in situ}} = 0.9013 (\text{pH}_{\text{NBS in situ}}) + 0.6905$ ($r^2 = 0.998$).

ORP sensor. The PMEL ORP sensor has a platinum working electrode and an Ag/AgCl reference electrode located in a single PEEK thermoplastic body. ORP sensor range is -500 to $+500$ millivolts, with output scaled to 0 – 5 volts for an auxiliary analog channel on the CTD. PMEL ORP sensor does not provide an Eh measurement, however, the sensors respond instantaneously to the presence of reduced chemical species with a decrease in the measured electric potential³⁷. ORP data are expressed as a time derivative ($\delta(\text{orp})/\delta t$), and anomalies are identified by negative values. This sensor provides a relative measure and no calibration is needed.

pH_{T,25}. The pH was measured on the total scale at a constant temperature of $25\text{ }^{\circ}\text{C}$ (pH_{T,25}) by the UV-Vis spectrophotometric technique³⁸ that used m-cresol purple as an indicator³⁹. The standard deviation for the measurements was ± 0.002 .

Total dissolved inorganic carbon and total alkalinity. The total dissolved inorganic carbon (C_T) and total alkalinity (A_T) were determined with a VINDTA 3C system (Marianda, Germany) that used coulometry in order to determine the total dissolved inorganic carbon and differential potentiometry for the total alkalinity^{40,41}. The certified reference material for oceanic CO₂, CRMs batch #117 was used to test the performance of both the total inorganic carbon and total alkalinity, resulting in a precision of $\pm 1.0\ \mu\text{mol kg}^{-1}$ for both parameters.

References

- Baker, E. T., Massoth, G. J., Walker, S. L. & Embley, R. W. A method for quantitatively estimating diffuse and discrete hydrothermal discharge. *Earth Planet. Sci. Letters*, **118**, 235–249 (1993).
- Lavelle, J. W. & Wetzler, M. A. Diffuse venting and background contributions to chemical anomalies in a neutrally buoyant ocean hydrothermal plume. *J. Geophys. Res.* **104**, 3201–3209 (1999).
- Le Bris, N., Govenar, B., Le Gall, C. & Fisher, C. R. Jr. Variability of physico-chemical conditions in $9^{\circ}50'$ N EPR diffuse flow vent habitats. *Mar. Chem.* **98**, 167–182 (2006).
- Walker, B. D., McCarthy, M. D., Fisher, A. T. & Guilderson, T. P. Dissolved inorganic carbon isotopic composition of low-temperature axial and ridge-flank hydrothermal fluids of the Juan de Fuca Ridge. *Mar. Chem.* **108**, 123–136 (2008).
- Wankel, S. D. *et al.* Influence of subsurface biosphere on geochemical fluxes from diffuse hydrothermal fluids. *Nature Geos.* **4**, 461–468 (2011).
- Hautala, S. *et al.* Low-temperature hydrothermal plumes in the near-bottom boundary layer at Endeavour Segment, Juan de Fuca Ridge. *Oceanog.* **25**, 192–195 (2012).
- Bemis, K., Lowell, R. P. & Farough, A. Diffuse flow on and around hydrothermal vents at mid-ocean ridges. *Oceanog.* **25**, 182–191 (2012).
- Elderfield, H. & Schultz, A. Mid-ocean ridge hydrothermal fluxes and the chemical composition of the ocean. *An. Rev. Earth Planet. Sci.* **24**, 191–224 (1996).
- Cardigos, F. *et al.* Shallow water hydrothermal vent field fluids and communities of the D. João de Castro Seamount (Azores). *Chem. Geol.* **224**, 153–168 (2005).
- Glasby, G. P. Direct observations of columnar scattering associated with geothermal gas bubbling in the Bay of Plenty, New Zealand. *J. Mar. Freshw. Res.* **5**, 483–496 (1971).
- Lyon, G. L., Giggenbach, W. F., Singleton, R. J. & Glasby, G. P. Isotopic and chemical composition of submarine geothermal gases from the Bay of Plenty. *Bull. N. Z. Dept. Sci. Ind. Res.* **218**, 65–67 (1977).
- Tarasov, V. G. *et al.* Effect of shallow-water hydrothermal venting on the biota of Matupi Harbour (Rabaul Caldera, New Britain Island, Papua New Guinea). *Cont. Shelf Res.* **19**, 79–116 (1999).
- Ólafson, J. *et al.* Initial observations, bathymetry and photography of a geothermal site on the Kolbeinsey Ridge. (eds Ayala-Castañares, A. *et al.*) 121–127 (Oceanography UNAM Press, 1988).
- Dando, P. R. *et al.* Gas venting rates from submarine hydrothermal areas around the island of Milos, Hellenic Volcanic Arc. *Cont. Shelf Res.* **15**, 913–929 (1995).
- Calanchi, N. *et al.* Submarine gas-emission from Panarea Island (Aeolian Archipelago): distribution of inorganic and organic compounds and inference about source conditions. *Acta Vulcanol.* **7**, 43–48 (1995).
- de Ronde, C. E. J. *et al.* Intra-oceanic subduction-related hydrothermal venting, Kermadec volcanic arc, New Zealand. *Earth Planet. Sci. Lett.* **193**, 359–369 (2001).
- Lupton, J. *et al.* Sub-marine venting of liquid carbon dioxide on a Mariana arc volcano. *Geochem. Geophys. Geosyst.* **7**, Q08007, doi: 10.1029/2005GC001152 (2006).
- Embley, R. W. *et al.* Long-term eruptive activity at a submarine arc volcano. *Nature* **441**, 494–497 (2006).
- Resing, J. *et al.* Chemistry of hydrothermal plumes above submarine volcanoes of the Mariana Arc. *Geochem., Geophys. Geosyst.* **10**(2), doi: 10.1029/2008GC002141 (2009).
- Tsunogai, U. *et al.* Peculiar features of Suiyo seamount hydrothermal fluids, Izu-Bonin Arc: Differences from subaerial volcanism. *Earth Planet. Sci. Lett.* **126**, 289–301 (1994).
- Michard, A. *et al.* Submarine thermal springs associated with young volcanoes: The Teahitia vents, Society Islands, Pacific Ocean. *Geochim. Cosmochim. Acta* **57**, 4977–4986 (1993).
- Sansone, F. J. & Resing, J. A. Hydrography and geochemistry of sea-surface hydrothermal plumes resulting from Hawaiian coastal volcanism. *J. Geophys. Res.* **100**, 13555–13569 (1995).
- Wheat, C. G. *et al.* Continuous sampling of hydrothermal fluids from Loihi Seamount after the 1996 event. *J. Geophys. Res.* **105**, 19353–19367 (2000).
- Staudigel, H. *et al.* Hydrothermal venting at Vaialulu'u Seamount: The smoking end of the Samoan chain. *Geochem. Geophys. Geosyst.* **5**, Q02003 (2004).
- Carracedo, J. C. *et al.* Hotspot volcanism close to a passive continental margin: The Canary Islands. *Geol. Magaz.* **135**, 591–604 (1998).
- Carracedo, J. C. *et al.* Cenozoic volcanism II: The Canary Islands (eds Gibbons, W. & Moreno, T.) 439–472 (Geological Society of London, 2002).
- Guillou, H., Carracedo, J. C., Pérez-Torrado, F. & Rodríguez Badiola, E. K-Ar ages and magnetic stratigraphy of a hotspot-induced, fast-grown oceanic island: El Hierro, Canary Islands. *J. Vol. Geo. Res.*, v. **73**, p. 141–155 (1996).
- Masson, D. G. Catastrophic collapse of the flank of El Hierro about 15,000 years ago, and the history of large flank collapses in the Canary Islands. *Geol.* **24**, 231–234 (1996).
- Zaczek, K. *et al.* Nannofossils in 2011 El Hierro eruptive products reinstate plume model for Canary Islands. *Sci. Rep.* **5**, doi: 10.1038/srep07945, (2015).
- Fraile-Nuez, E. *et al.* The submarine volcano eruption at the island of El Hierro: physical-chemical perturbation and biological response. *Sci. Rep.* **2**, doi: 10.1038/srep00486 (2012).

31. Santana-Casiano, J. M. *et al.* The natural ocean acidification and fertilization event caused by the submarine eruption of El Hierro. *Sci. Rep.* **3**. doi: 10.1038/srep01140 (2013).
32. Baker, E. T. *et al.* Hydrothermal cooling along the Eastern Lau Spreading Center: No evidence for discharge beyond the neovolcanic zone. *Geochem. Geophys. Geosyst.* **11**, Q08004, doi: 10.1029/2010GC003106 (2010).
33. Egbert, G. D., Bennett, A. F. & Foreman, M. G. TOPEX/POSEIDON tides estimated using a global inverse model. *J. Geophys. Res.* **99**, 24821–24852 (1994).
34. Dziak, R. P. *et al.* Flux measurements of explosive degassing using a yearlong hydroacoustic record at an erupting submarine volcano. *Geochem. Geophys. Geosyst.* **13**, Q0AF07, doi:10.1029/2012GC004211 (2012).
35. Marty, B. & Tolstikhin, I. N. CO₂ fluxes from mid-ocean ridges, arcs and plumes. *Chem. Geol.* **145**, 233–248 (1998).
36. Le Quéré, C. *et al.* Global Carbon Budget 2015. *Earth Syst. Sci. Data* **7**. doi: 10.5194/essd-7 (2015).
37. Walker, S. L. *et al.* A new tool for detecting hydrothermal plumes: an ORP sensor for the PMEL MAPR. Fall Meeting Supplement, Abstract V21D-0753 EOS, *Transact. Am. Geophys. U.* **88**, 52 (2007).
38. Clayton, T. D. & Byrne, R. H. Spectrophotometric seawater pH measurements: total hydrogen ion concentration scale calibration of m-cresol purple and at-sea results, *Deep-Sea Res.* **140**, 2115–2129 (1993).
39. González-Dávila, M. *et al.* Seasonal and interannual variability of sea surface carbon dioxide species at the European Station for Time Series in the Ocean at the Canary Islands (ESTOC) between 1996 and 2000, *Global Biogeochem. Cycles* **17**, 1076 (2003).
40. Dickson, A. G., Sabine, C. L. & Christian, J. R. (eds). Guide to best practice for ocean CO₂ measurements. *PICES Special Publication* **3**, 191 (2007).
41. Mintrop, L. *Versatile instruments for the determination of titration alkalinity. Manual for versions 3S and 3C. Version 2.0*, MARine ANalytics and DATA (MARIANDA), Kiel, Germany, 45 (2004).

Acknowledgements

This study has been supported by funds from FEDER and the Spanish Ministry of Economy and Competitiveness through the VULCANO project (CTM2012-36317). The authors would like to thank the invaluable work of the officers and crew of the R/V *Ángeles Alvariño* from the Spanish Institute of Oceanography. ETB, JAR, and SLW were supported by the NOAA/PMEL Earth-Ocean Interactions Program and the Joint Institute for the Study of the Atmosphere and Ocean (JISAO) under NOAA Cooperative Agreement No. NA10OAR4320148. PMEL contribution 4397, JISAO contribution 2471.

Author Contributions

Observational data was provided by J.M.S.-C., E.F.-N. and M.G.-D. All the authors participated in the data analysis, interpretation of the results and writing.

Additional Information

Supplementary information accompanies this paper at <http://www.nature.com/srep>

Competing financial interests: The authors declare no competing financial interests.

How to cite this article: Santana-Casiano, J. M. *et al.* Significant discharge of CO₂ from hydrothermalism associated with the submarine volcano of El Hierro Island. *Sci. Rep.* **6**, 25686; doi: 10.1038/srep25686 (2016).



This work is licensed under a Creative Commons Attribution 4.0 International License. The images or other third party material in this article are included in the article's Creative Commons license, unless indicated otherwise in the credit line; if the material is not included under the Creative Commons license, users will need to obtain permission from the license holder to reproduce the material. To view a copy of this license, visit <http://creativecommons.org/licenses/by/4.0/>